Dinuclear Nickel(II) Complexes of Phenol-Based "End-Off" Compartmental Ligands and Their Urea Adducts Relevant to the Urease Active Site

Takeichiro Koga, Hideki Furutachi, Takako Nakamura, Nobuo Fukita, Masaaki Ohba, Kazuhiro Takahashi, and Hisashi Ōkawa*

Department of Chemistry, Faculty of Science, Kyushu University, Hakozaki, Higashiku, Fukuoka 812, Japan

Received September 19, 1997

Two phenol-based compartmental ligands of the "end-off" type, 2,6-bis{*N*-[2-(dimethylamino)ethyl]iminomethyl}-4-methylphenol (HL^1) and 2-{*N*-[2-(dimethylamino)ethyl]iminomethyl}-6-{*N*-methyl-*N*-[2-(dimethylamino)ethyl]-aminomethyl}-4-bromophenol (HL^2), have been used to form $[Ni_2(L^1)(AcO)(NCS)_2(MeOH)]$ (**1**), $[Ni_2(L^1)(AcO)_2(MeOH)]BPh_4$ (**2**), $[Ni_2(L^2)(AcO)(NCS)_2(MeOH)]$ (**3**), $[Ni_2(L^2)(AcO)_2]BPh_4$ (**4**), and $[Ni_2(L^2)(NCS)_3(MeOH)]$ (**5**). X-ray crystallographic studies were done for **2**−**5**. **2**: triclinic, space group $P\bar{1}$, $a = 13.613(3)$ Å, $b = 16.475(4)$ Å, $c = 11.307(4)$ Å, $\alpha = 99.90(2)°$, $\beta = 104.16(2)°$, $\gamma = 109.01(2)°$, $V = 2253(1)$ Å^3, $Z = 2$. The complex cation has a dinuclear core triply bridged by the phenolic oxygen of $(L^1)^-$ and two acetate groups in the syn-syn mode. One Ni has a six-coordinate geometry together with a methanol oxygen. **3**: triclinic, space group $P\bar{1}$, $a = 10.167(1)$ Å, $b = 16.119(2)$ Å, $c = 9.472(3)$ Å, $\alpha = 103.53(2)°$, β=100.91(1)°, $\gamma = 85.62(1)°$, $V = 1481(1)$ Å^3, $Z = 2$. A pair of Ni ions are bridged by the phenolic oxygen of $(L^2)^-$, an isothiocyanate nitrogen, and an acetate group. The sixth position of one Ni is occupied by a methanol oxygen and that of the other Ni by isothiocyanate nitrogen. **4**: monoclinic, space group $P2_1/n$, $a = 15.146(2)$ Å, $b = 9.442(3)$ Å, $c = 30.844(2)$ Å, $\beta = 93.427(9)°$, $V = 4402(1)$ Å^3, $Z = 4$. Two Ni ions are bridged by the phenolic oxygen of $(L^2)^-$ and an acetate group. The Ni bound to the iminic pendant arm is nearly planar whereas the Ni bound to the aminic pendant arm is of six-coordination together with a bidentate acetate group. **5**: monoclinic, space group $C2/c$, $a = 26.744(5)$, $b = 10.323(4)$ Å, $c = 21.785(6)$ Å, $\beta = 94.73(2)°$, V = 5993(3) Å^3, $Z = 8$. Two Ni ions are bridged by the phenolic oxygen of $(L^2)^-$ and an isothiocyanate nitrogen. The Ni bound to the iminic pendant arm is of five-coordination along with an isothiocyanate nitrogen. The Ni bound to the aminic pendant arm has a six-coordinate geometry together with a methanol oxygen and an isothiocyanate nitrogen. **1**−**5** were examined regarding their ability to bind urea, and **4** and **5** were shown to form $[Ni_2(L^2)(AcO)_2(urea)]BPh_4$ (**4′**) and $[Ni_2(L^2)(NCS)_3(urea)]$ (**5′**), respectively. **5′** crystallizes in the monoclinic system, space group $P2_1/n$, with $a = 11.709(5)$, $b = 15.100(4)$, $c = 17.548(5)$ Å, $\beta = 95.58(3)°$, $V = 3087(1)$ Å^3, and $Z = 4$. Its dinuclear core is very similar to that of **5** except that the methanol of **5** is replaced by a urea molecule.

Introduction

Urease is a nickel-dependent metalloenzyme that catalyzes the hydrolysis of urea to ammonia and carbon dioxide,[1] in conjunction with biological functions using urea as a nitrogen source.[2] It was first isolated from jack beans in 1926[3] and later from various origins such as bacteria, fungi, and plants.[1] A recent X-ray crystallographic study on microbial urease from *Klebsiella aerogenes* has identified a dinickel active site.[4] The two nickel ions are bridged by a carboxylate group of a carbamylated lysine residue with a Ni--Ni separation of 3.5 Å. The geometrical structure around one nickel (Ni1) is pseudo-tetrahedral with two histidine nitrogens, an oxygen of the carbamate bridge, and a water molecule; the fourth position is only partially occupied by a water molecule and considered to be a likely candidate for binding urea in the catalysis. The geometry around another nickel (Ni2) is depicted as trigonal bipyramidal with further coordination of an asparagine oxygen. It is considered that urease employs a nonequivalent pair of nickel ions to facilitate the concerted binding of the substrate at one center and nucleophilic attack of water or hydroxide at the other center.[5,6] It is noted that the water attached to Ni2 is situated close to Ni1, suggesting a possible formation of a (μ-hydroxo)(μ-carboxylato)dinickel core under physiological conditions. Such dinuclear cores bridged by one oxygenic ligand (oxo, hydroxo, or water) and one or two carboxylate groups are widely known in metallobiosites.[7] Some urease models are provided[8−13] and urea adducts of dinickel complexes are

(1) Hausinger, R. P. *Biochemistry of Nickel*; Plenum Press: New York, 1993; Chapter 12, pp 23−50.
(2) Mobley, H. L. T.; Hausinger, R. P. *Microbiol. Rev.* **1989**, *53*, 85.
(3) Sumner, J. B. *J. Biol. Chem.* **1926**, *69*, 435.
(4) Jabri, E.; Carr, M. B.; Hausinger, R. P.; Karplus, P. A. *Science* **1995**, *268*, 998.
(5) Dixon, N. E.; Riddles, P. W.; Gazzola, C.; Blakeley, R. L.; Zerner, B. *Can. J. Biochem.* **1980**, *58*, 1335.
(6) Lippard, S. J. *Science* **1995**, *268*, 996.
(7) Fenton D. E.; Okawa, H. In *Perspectives on Bioinorganic Chemistry, Vol. 2*; Hay, R. W., Dilworth, J. R., Nolan, K. B., Eds.; JAI Press: London, 1993; pp 81−138.
(8) Chaudhuri, P.; Küppers, H.-J.; Wieghardt, K.; Gehring, S.; Haase, H.; Nuber, B.; Weiss, J. *J. Chem. Soc., Dalton Trans.* **1988**, 1367.
(9) Buchanan, R. M.; Mashuta, M. S.; Oberhausen, K. J.; Richardson, J. F.; Li, Q.; Hendrickson, D. N. *J. Am. Chem. Soc.* **1989**, *111*, 4497.
(10) Wages, H. E.; Taft, K. L.; Lippard, S. L. *Inorg. Chem.* **1993**, *32*, 4985.
(11) Stemmler, A. J.; Kamph, J. W.; Kirk, M. L.; Pecoraro, V. L. *J. Am. Chem. Soc.* **1995**, *117*, 6368.
(12) Volkmer, D.; Hörstmann, A.; Griesar, K.; Haase, W.; Krebs, B. *Inorg. Chem.* **1996**, *35*, 1132.

S0020-1669(97)01209-3 CCC: $15.00
Published on Web 02/12/1998

Chart 1. Chemical Structures of $(L^1)^-$ and $(L^2)^-$

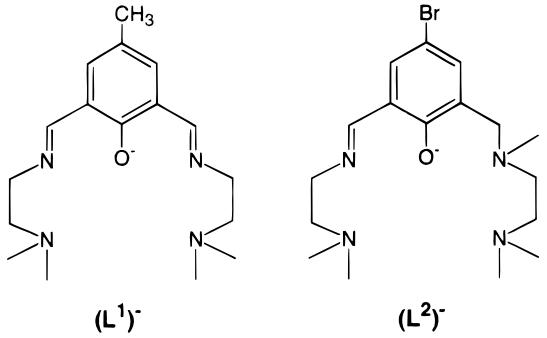

reported.[10] Recently, catalytic ethanolysis of urea by a (μ-alkoxo)(μ-carboxylato)dinickel(II) complex was was reported.[14]

To provide further analogues of the urease active site, we have studied dinuclear nickel complexes derived from two phenol-based end-off compartmental ligands, 2,6-bis{*N*-[2-(dimethylamino)ethyl]iminomethyl}-4-methylphenol (HL^1)[15] and 2-{*N*-[2-(dimethylamino)ethyl]iminomethyl}-6-{*N*-methyl-*N*-[2-(dimethylamino)ethyl]aminomethyl}-4-bromophenol (HL^2):[16] $[Ni_2(L^1)(AcO)(NCS)_2(MeOH)]$ (**1**), $[Ni_2(L^1)(AcO)_2(MeOH)]BPh_4$ (**2**), $[Ni_2(L^2)(AcO)(NCS)_2(MeOH)]$ (**3**), $[Ni_2(L^2)(AcO)_2]BPh_4$ (**4**), and $[Ni_2(L^2)(NCS)_3(MeOH)]$ (**5**). The chemical structures of HL^1 and HL^2 are shown in Chart 1. The crystal structure analyses for **2**−**5** indicate a phenoxo-bridged dinuclear core structure in a geometric asymmetry. It is found that **4** accommodates a urea molecule at the four-coordinate nickel to give $[Ni_2(L^2)(AcO)_2(urea)]BPh_4$ (**4′**). Further, the methanol ligand in **5** is substituted by urea to give $[Ni_2(L^2)(NCS)_3(urea)]$ (**5′**), whose crystal structure is determined by X-ray crystallography.

Experimental Section

Measurements. Elemental analyses of C, H, and N were obtained at the Elemental Analysis Service Center of Kyushu University. Analyses of Ni were obtained using a Shimadzu AA-660 atomic absorption/flame emission spectrophotometer. Infrared spectra were recorded on a JASCO IR-810 spectrometer using KBr disks. Molar conductances were measured at $\sim 1 \times 10^{-3}$ M concentration using a DKK AOL-10 conductivity meter at 20 °C. Electronic spectra were recorded on a Shimadzu MPS-2000 spectrometer. Magnetic susceptibilities were determined on a Faraday balance in the temperature range 80−300 K and on a HOXAN HSM-D SQUID susceptometer in the range 4.2−80 K. Calibrations were done using $[Ni(en)_3]S_2O_3$.[17] Effective magnetic moments were calculated by the equation $\mu_{eff} = 2.828(\chi_A T)^{1/2}$, where χ_A is the magnetic susceptibility per nickel corrected for the diamagnetism of the constituent atoms using Pascal's constants.[18]

Material. Unless otherwise stated, all reagents were purchased from commercial sources and used without further purification. Solvents were dried by standard methods. 2,6-Diformyl-4-methylphenol[19] and 3-{*N*-methyl-*N*-(2-dimethylamino)ethyl}aminomethyl-5-bromosalicylaldehyde[16] were prepared by literature methods.

Preparation of Nickel Complexes. (a) $[Ni_2(L^1)(AcO)(NCS)_2(MeOH)]$ (1). A solution of 2,6-diformyl-4-methylphenol (0.164 g, 1.0 mmol) and *N*,*N*-dimethylethylenediamine (0.176 g, 2.0 mmol) in methanol (5 cm^3) was refluxed for 10 min. To the resulting yellow solution of HL^1 was added nickel(II) acetate tetrahydrate (0.498 g, 2.0 mmol), and the mixture was refluxed for 30 min. The addition of sodium thiocyanate (0.162 g, 2.0 mmol) resulted in the precipitation of green microcrystals. Yield: 0.310 g (49.3%). Anal. Found: C, 42.08; H, 5.53; N, 13.27; Ni, 18.4. Calcd for $C_{22}H_{34}N_6Ni_2O_4S_2$: C, 42.07; H, 5.46; N, 13.38; Ni, 18.7. Selected IR data (ν/cm^{-1}) using KBr disk: 3000−2800, 2080, 2020, 1660, 1570, 1540, 1460. Molar conductance: nonelectrolyte in CH_2Cl_2. Visible spectral data [λ/nm (ϵ/$M^{-1}cm^{-1}$)] in CH_2Cl_2: 610 (53), 780 (30), 880 (65).

(b) $[Ni_2(L^1)(AcO)_2(MeOH)]BPh_4$ (2). This complex was prepared as green microcrystals by a method similar to that for **1** except for the use of sodium tetraphenylborate instead of sodium thiocyanate. Yield: 80.4%. Anal. Found: C, 62.33; H, 6.35; N, 6.38; Ni, 12.9. Calcd for $C_{46}H_{57}BN_4Ni_2O_6$: C, 62.07; H, 6.45; N, 6.29; Ni, 13.4. Selected IR data (ν/cm^{-1}) using KBr disk: 3520, 3050−2800, 1640, 1600, 1550, 1430, 740, 720. Molar conductance (Λ_M/S cm^2 mol^{-1}) in CH_2Cl_2: 46. Visible spectral data [λ/nm (ϵ/M^{-1} cm^{-1})] in CH_2Cl_2: 655 (58), 780 (25), 880 (65).

(c) $[Ni_2(L^2)(AcO)(NCS)_2(MeOH)]$ (3). A solution of 5-bromo-3-{*N*-[2-(dimethylamino)ethyl]-*N*-methyl}aminomethylsalicylaldehyde (0.314 g, 1.0 mmol) and *N*,*N*-dimethylethylenediamine (0.088 g, 1.0 mmol) in methanol (5 cm^3) was refluxed for 10 min. To the resulting yellow solution of HL^2 was added nickel(II) acetate tetrahydrate (0.498 g, 2.0 mmol), and the mixture was refluxed for 30 min. The addition of sodium thiocyanate (0.162 g, 2.0 mmol) resulted in the precipitation of green microcrystals. Yield: 0.320 g (45.2%). Anal. Found: C, 37.34; H, 5.07; N, 11.70; Ni, 16.7. Calcd for $C_{22}H_{35}BrN_6Ni_2O_4S_2$: C, 37.27; H, 4.98; N, 11.85; Ni, 16.6. Selected IR data (ν/cm^{-1}) using KBr disk: 3520, 3000−2800, 2075, 2025, 1650, 1580, 1550, 1450. Molar conductance: nonelectrolyte in CH_2Cl_2. Visible spectral data [λ/nm (ϵ/M^{-1} cm^{-1})] in CH_2Cl_2: 615 (45), 780 (20), 875 (40).

(d) $[Ni_2(L^2)(AcO)_2]BPh_4$ (4). This was prepared as a brown powder by a method similar to that for **3** using sodium tetraphenylborate instead of sodium thiocyanate. Yield: 56.4%. Anal. Found: C, 57.50; H, 5.80; N, 5.90; Ni, 12.9. Calcd for $C_{45}H_{54}BrN_4Ni_2O_5$: C, 57.56; H, 5.80; N, 5.97; Ni, 12.5. Selected IR data (ν/cm^{-1}) using KBr disk: 3050−2800, 1630, 1580, 1550, 1450, 740, 710. Molar conductance (Λ_M/S cm^2 mol^{-1}) in CH_2Cl_2:45. Visible spectral data [λ/nm (ϵ/M^{-1} cm^{-1})] in CH_2Cl_2: ∼500 (sh), 625 (40), 780 (25), 865 (25).

(e) $[Ni_2(L^2)(NCS)_3(MeOH)]$ (5). This was obtained as a green precipitate in a manner similar to that for **3**, using nickel(II) thiocyanate instead of nickel(II) acetate tetrahydrate and sodium thiocyanate. Yield: 49.3%. Anal. Found: C, 35.64; H, 4.57; N, 13.80; Ni, 16.6. Calcd for $C_{21}H_{32}BrN_7Ni_2O_2S$: C, 35.64; H, 4.56; N, 13.85; Ni, 16.6. Selected IR data (ν/cm^{-1}) using KBr disk: 3000−2800, 2080, 1980, 1650. Molar conductance: nonelectrolyte in CH_2Cl_2. Visible spectral data [λ/nm (ϵ/M^{-1} cm^{-1})] in CH_2Cl_2: 660 (70), 785 (35), 890 (45).

Preparation of Urea Adducts. (a) $[Ni_2(L^2)(AcO)_2(urea)]BPh_4$ (4′). To a solution of **4** (0.47 g, 0.5 mmol) in dichloromethane (5 cm^3) was added powdered urea (excess), and the mixture was stirred for 1 h. Unreacted urea was removed by filtration, and the resulting green solution was diffused with hexane to give green microcrystals. Yield: 0.395 g (78%). Anal. Found: C, 55.11; H, 5.87; N, 8.12; Ni, 12.3. Calcd for $C_{46}H_{58}BBrN_6Ni_2O_6$: C, 55.30; H, 5.85; N, 8.41; Ni, 11.8. Selected IR (ν/cm^{-1}) using KBr disk: 3550−3300, 3050−2800, 1660, 1580, 1550, 1450. Molar conductance (Λ_M/S cm^2 mol^{-1}) in CH_2Cl_2: 16. Visible spectral data [λ/nm(ϵ/M^{-1} cm^{-1})] in CH_2Cl_2: 625 (35), 780 (sh), 880 (25).

(b) $[Ni_2(L^2)(NCS)_3(urea)]$ (5′). This was obtained as green microcrystals by the reaction of **5** with excess urea in dichloromethane. Yield: 50%. Anal. Found: C, 34.18; H, 4.38; N, 16.99; Ni, 15.9. Calcd for $C_{21}H_{32}BrN_9Ni_2O_2S_3$: C, 34.27; H, 4.38; N, 17.13; Ni, 15.9. Selected IR data (ν/cm^{-1}) using KBr disk: 3600−3200, 3050−2750, 2100, 1990, 1650, 1640, 1610, 1590. Molar conductance (Λ_M/S cm^2 mol^{-1}) in CH_2Cl_2: nonelectrolyte. Visible spectral data [λ/nm (ϵ/M^{-1} cm^{-1})] in CH_2Cl_2: 655 (58), 780 (40), 880 (50).

(13) Volkmer, D.; Hommerich, B.; Griesar, K.; Haase, W.; Krebs, B. *Inorg. Chem.* **1996**, *35*, 3792.
(14) Yamaguchi, K.; Koshino, S.; Akagi, F.; Suzuki, M.; Uehara, A.; Suzuki, S. *J. Am. Chem. Soc.* **1997**, *119*, 5752.
(15) Sakiyama, H.; Tamaki, H.; Kodera, M.; Matsumoto, N.; Ōkawa, H. *J. Chem. Soc., Dalton Trans.* **1993**, 591.
(16) Higuchi, C.; Sakiyama, H.; Ōkawa, H.; Isobe, R.; Fenton, D. E. *J. Chem. Soc., Dalton Trans.* **1994**, 1097.
(17) Curtis, N. F. *J. Chem. Soc.* **1961**, 3147.
(18) Boudreaux, E. A.; Mulay, L. N. *Theory and Applications of Molecular Paramagnetism*; Wiley: New York, 1976; pp 491−494.
(19) Denton, D. A.; Suschitzky, H. *J. Chem. Soc.* **1963**, 4741.

Table 1. Crystallographic Data for **2**, **3**, **4**, **5**, and **5′**

	2	**3**	**4**	**5**	**5′**
formula	$C_{46}H_{57}BN_4Ni_2O_6$	$C_{22}H_{35}BrN_5Ni_2O_4S_2$	$C_{45}H_{54}BBrN_4Ni_2O_5$	$C_{21}H_{32}BrN_7Ni_2O_2S_3$	$C_{21}H_{32}BrN_9Ni_2O_2S_3$
crystal color	green	green	brown	green	green
fw	890.19	708.98	939.06	708.01	736.03
crystal size, mm	0.20 × 0.30 × 0.03	0.25 × 0.15 × 0.30	0.20 × 0.20 × 0.25	0.60 × 0.40 × 0.30	0.20 × 0.20 × 0.10
crystal system	triclinic	triclinic	monoclinic	monoclinic	monoclinic
space group	$P\bar{1}$	$P\bar{1}$	$P2_1/n$	$C2/c$	$P2_1/c$
a, Å	13.613(3)	10.167(1)	15.146(2)	26.744(5)	11.709(5)
b, Å	16.475(4)	16.119(2)	9.442(3)	10.323(4)	15.100(4)
c, Å	11.307(4)	9.472(3)	30.844(2)	21.785(6)	17.548(5)
α, deg	99.90(2)	103.53(2)	90	90	90
β, deg	104.16(2)	100.91(1)	93.427(9)	94.73(2)	95.58(3)
γ, deg	109.01(2)	85.62(1)	90	90	90
V, Å^3	2235(1)	1481.2(5)	4402(1)	5993(3)	3087(1)
Z	2	2	4	8	4
D_{calcd}, g cm^{-3}	1.322	1.589	1.417	1.569	1.583
λ(Mo Kα), Å	0.710 69	0.710 69	0.710 69	0.710 69	0.710 69
no. of reflns	7878	5532	8597	5734	5953
R^a	0.055	0.050	0.063	0.067	0.041
$R_w{}^{b,c}$	0.047	0.054	0054	0.051	10.1

[a] $R = \sum||F_o| - |F_c||/\sum|F_o|$. [b] $R_w = \{\sum[w(|F_o| - |F_c|)^2]/\sum[w|F_o|^2]\}^{1/2}$. [c] $w = 1/\sigma^2(F_o)$.

Crystal Structure Analyses. Single crystals of **2**, **3**, and **5** were obtained by crystallization from methanol. Single crystals of **4** and **5′** were grown from a 2-propanol/dichloromethane (1:1 in volume) mixture. Each crystal of **2**, **3**, **4**, and **5′** was coated with epoxy resin, and a crystal of **5** was sealed in a glass tube. Intensities and lattice parameters were obtained on a Rigaku AFC-7R automated four-circle diffractometer, using graphite-monochromated Mo Kα radiation (λ = 0.710 69 Å) and a 12 kW rotating anode generator at 20 ± 1 °C. The cell parameters were determined by 25 reflections in the 2θ ranges 29.33° < 2θ < 29.96° for **2**, 29.49° < 2θ < 29.98° for **3**, 27.79° < 2θ < 29.64° for **4**, 29.57° < 2θ < 29.97° for **5**, and 6.94° < 2θ < 14.51° for **5′**. For the intensity data collections, the $\omega-2\theta$ scan mode was used to a maximum 2θ value of 50.0°. The scan rates were 16° min^{-1} for **2**−**5** and 8° min^{-1} for **5′**. The weak reflections ($I < 10.0\sigma(I)$) were rescanned (maximum of four scans), and the counts were accumulated to ensure good counting statistics. Stationary-background counts were recorded on each side of the reflection. The ratio of peak counting time to background counting time was 2:1. The diameter of the incident-beam collimator was 1.0 mm, the crystal to detector distance was 235 mm, and the computer-controlled detector aperture was set to 9.0 × 13.0 mm (horizontal × vertical). Three standard reflections were monitored every 150 reflections. Over the course of data collection, the standards decreased by 7.22% for **2**, increased by 1.35% for **3**, decreased by 3.24% for **4**, increased by 0.7% for **5**, and decreased by 0.8% for **5′**. A linear correction factor was applied to the data to account for the phenomena. The linear absorption coefficients, μ, for Mo Kα radiation were 8.9 cm^{-1} for **2**, 14.0 cm^{-1} for **3**, 18.1 cm^{-1} for **4**, 28.3 cm^{-1} for **5**, and 27.6 cm^{-1} for **5′**. An empirical absorption correction based on azimuthal scans of several reflections was applied which resulted in transmission factors ranging from 0.88 to 1.00 for **2**, from 0.62 to 1.00 for **3**, from 0.89 to 1.00 for **4**, from 0.77 to 1.00 for **5**, and from 0.89 to 1.00 for **5′**. The intensity data were corrected for Lorentz and polarization factors. A correction for secondary extinction was applied (coefficients: 2.398 20 × 10^{-7} for **2**, 1.900 028 × 10^{-7} for **3**, 3.165 72 × 10^{-7} for **4**, 5.689 42 × 10^{-7} for **5**, and 8.158 92 × 10^{-7} for **5′**). Crystal data parameters for **2**, **3**, **4**, **5**, and **5′** are summarized in Table 1.

The structures were solved by direct methods and expanded using Fourier techniques. Refinements were carried out by the full-matrix least-squares methods, where the function minimized was $\sum w(|F_o| - |F_c|)^2$ with $w = 1/\sigma^2(F_o)$. Non-hydrogen atoms were refined anisotropically. Hydrogen atoms were fixed at the calculated positions and were not refined.

Neutral-atom scattering factors were taken from Cromer and Waber.[20] Anomalous dispersion effects were included in F_c; the values for $\Delta f'$ and $\Delta f''$ were those of Creagh and McAuley.[21] The values for the mass attenuation coefficients were those of Creagh and Hubbell.[22] All calculations were performed using the teXsan crystallographic software package[23] of the Molecular Structure Corp.

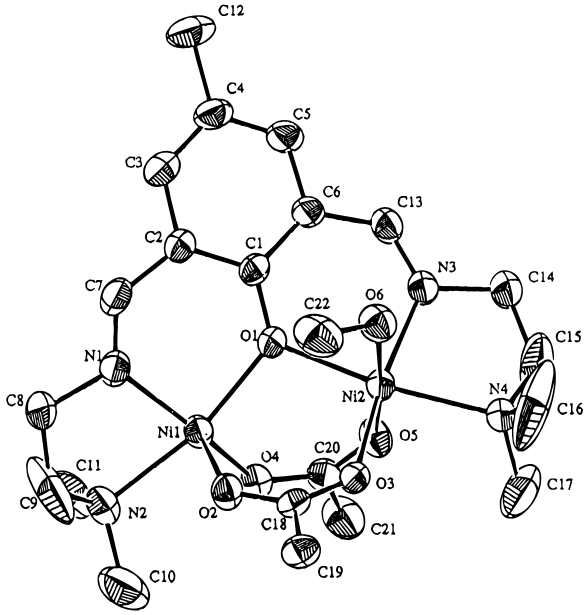

Figure 1. ORTEP view of $[Ni_2(L^1)(AcO)_2(MeOH)]BPh_4$ (**2**).

Results and Discussion

Crystal Structures of Complexes 2−5. Complex 2. An ORTEP[24] view of $[Ni_2(L^1)(AcO)_2(MeOH)]BPh_4$ (**2**) is shown in Figure 1 together with the numbering scheme. Selected bond distances and angles are given in Table 2.

The complex has a dinuclear core bridged by the phenolic oxygen of $(L^1)^-$ and two acetate groups in the syn-syn mode, providing a (μ-phenoxo)bis(μ-carboxylato)dinickel(II) core in the Ni--Ni separation of 3.311(1) Å. A methanol molecule

(20) Cromer, D. T.; Waber, J. T. *International Tables for X-ray Crystallography;* Kynoch Press: Birmigham, U.K., 1974; Vol. IV.

(21) Creagh, D. C.; McAuley, W. J. *International Tables for Crystallography*, Kluwer: Boston, MA, 1992; pp 219−222.

(22) Creagh, D. C.; Hubbell, H. H. *International Tables for Crystallography*; Kluwer: Boston, MA, 1992; pp 200−206.

(23) *teXsan*, Molecular Structure Corp.: Houston, TX, 1985.

(24) Johnson, C. K. *ORTEP*; Report 3794; Oak Ridge National Laboratory: Oak Ridge, TN, 1965.

Table 2. Relevant Bond Distances (Å) and Angles (deg) for **2**

Distances			
Ni1−O1	2.022(3)	Ni1−O2	1.982(3)
Ni1−O4	1.973(3)	Ni1−N1	1.983(4)
Ni1−N2	2.138(4)	Ni2−O1	2.044(3)
Ni2−O3	2.006(3)	Ni2−O5	2.037(3)
Ni2−O6	2.270(4)	Ni2−N3	2.002(4)
Ni1--Ni2	3.311(1)		
Angles			
O1−Ni1−O2	98.8(1)	O1−Ni1−O4	96.2(1)
O1−Ni1−N1	89.2(2)	O1−Ni1−N2	167.1(2)
O2−Ni1−O4	103.9(1)	O2−Ni1−N1	97.3(2)
O2−Ni1−N2	91.5(2)	O4−Ni1−N1	157.0(2)
O4−Ni1−N2	88.7(2)	N1−Ni1−N2	81.8(2)
O1−Ni2−O3	97.8(1)	O1−Ni2−O5	91.1(1)
O1−Ni2−O6	84.8(1)	O1−Ni2−N3	89.8(2)
O1−Ni2−N4	171.3(2)	O3−Ni2−O5	96.8(1)
O3−Ni2−O6	83.9(1)	O3−Ni2−N3	167.2(2)
O3−Ni2−N4	90.9(1)	O5−Ni2−O6	175.9(1)
O5−Ni2−N3	93.3(2)	O5−Ni2−N4	87.8(2)
O6−Ni2−N3	86.6(2)	O6−Ni2−N4	96.3(2)
N3−Ni2−N4	81.6(2)	Ni1−O1−Ni2	109.1(1)

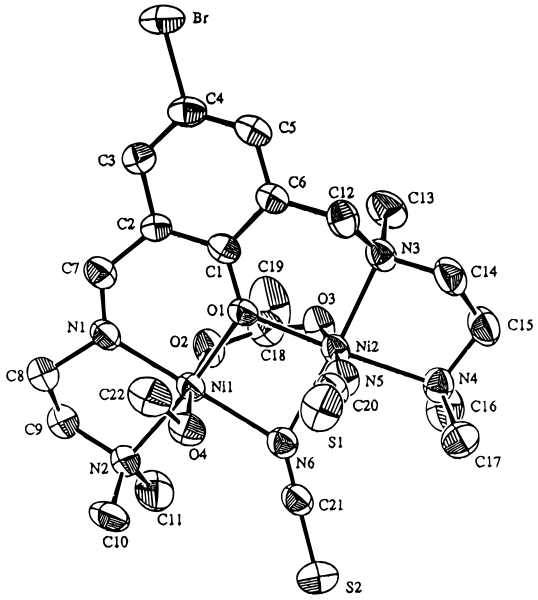

Figure 2. ORTEP view of $[Ni_2(L^2)(AcO)(NCS)_2(MeOH)]$ (**3**).

coordinates to one nickel, forming a geometrically asymmetric core with a {5/6} coordination number set. The geometry around the five-coordinate nickel (Ni1) is depicted as a square pyramid with N1, N2, and O1 of $(L^1)^-$ and O4 of one acetate bridge on the basal plane and O2 of another acetate bridge at the apex. The geometry around the six-coordinate nickel (Ni2) forms a distorted octahedron. The six-coordinate Ni2 has long metal-to-ligand bond distances (2.006(3)−2.270(4) Å) relative to the five-coordinate Ni1 (1.973(3)−2.022(3) Å). In particular, the Ni2−O6(methanol) bond distance (2.270(4) Å) is elongated. It must be mentioned that the core of this complex resembles that of $[Mn_2(L^1)(AcO)_2NCS]$,[15] where the sixth position of the six-coordinate manganese is occupied by the isothiocyanate nitrogen.

Complex 3. An ORTEP view of $[Ni_2(L^2)(AcO)(NCS)_2$-(MeOH)] (**3**) is shown in Figure 2 together with the numbering scheme. Selected bond distances and angles are given in Table 3.

X-ray crystallography has confirmed that a pair of nickel ions are bridged by the phenolic oxygen of $(L^2)^-$, an isothiocyanate nitrogen, and an acetate group in the syn-syn mode. The Ni1--Ni2 separation is 2.993(1) Å. The sixth position of one Ni

Table 3. Relevant Bond Distances (Å) and Angles (deg) for **3**

Distances			
Ni1−O1	2.027(4)	Ni1−O2	2.036(4)
Ni1−O4	2.180(4)	Ni1−N1	1.990(5)
Ni1−N2	2.143(5)	Ni1−N6	2.131(5)
Ni2−O1	2.042(4)	Ni2−O3	2.034(4)
Ni2−N3	2.113(5)	Ni2−N4	2.167(5)
Ni2−N5	2.105(6)	Ni2−N6	2.172(5)
Ni1--Ni2	2.993(1)		
Angles			
O1−Ni1−O2	91.1(2)	O1−Ni1−O4	84.4(2)
O1−Ni1−N1	89.7(2)	O1−Ni1−N2	173.5(2)
O2−Ni1−N6	86.9(2)	O2−Ni1−O4	172.2(2)
O2−Ni1−N1	93.0(2)	O2−Ni1−N2	90.5(2)
O2−Ni1−N6	93.0(2)	O4−Ni1−N1	93.3(2)
O4−Ni1−N2	94.7(2)	O4−Ni1−N6	80.4(2)
N1−Ni1−N2	83.9(2)	N1−Ni1−N6	173.1(2)
N2−Ni1−N6	99.3(2)	O1−Ni2−O3	90.5(2)
O1−Ni2−N3	91.6(1)	O1−Ni2−N4	175.8(2)
O1−Ni2−N5	85.0(2)	O1−Ni2−N6	85.4(2)
O3−Ni2−N3	89.9(2)	O3−Ni2−N4	92.1(2)
O3−Ni2−N5	173.9(2)	O3−Ni2−N6	87.7(2)
N3−Ni2−N4	85.3(2)	N3−Ni2−N5	94.3(2)
N3−Ni2−N6	176.2(2)	N4−Ni2−N5	92.6(2)
N4−Ni2−N6	97.9(2)	N5−Ni2−N6	87.8(2)
Ni1−O1−Ni2	94.7(2)	Ni1−N6−Ni2	88.1(2)

(Ni1) is occupied by a methanol oxygen (O4), and the sixth position of the other Ni (Ni2) is occupied by an isothiocyanate nitrogen (N5), giving a {6/6} coordination number set. The methanol molecule on Ni1 and the thiocyanate group on Ni2 are situated cis relative to each other with respect to the mean molecular plane. The equatorial plane about Ni1 is formed by N1 and N2 of the iminic pendant arm and O1 and N6 of the bridges. The equatorial plane about Ni2 is formed by N3 and N4 of the aminic pendant arm and O1 and N6 of the bridges. The two equatorial planes sharing O1 and N6 form a good coplane, and the acetate group bridges the two nickel ions at their axial sites. The Ni1-to-ligand bond distances fall in the range 1.990(5)−2.180(4) Å, whereas the Ni2-to-ligand bond distances fall in the smaller range 2.034(4)−2.172(5) Å. The Ni1−N1(imine) bond distance (1.990(5) Å) is fairly short relative to the Ni2−N3(amine) distance (2.113(5) Å).

Complex 4. An ORTEP view of $[Ni_2(L^2)(AcO)_2]BPh_4$ (**4**) is shown in Figure 3 together with the numbering scheme. Selected bond distances and angles are given in Table 4.

A pair of nickel ions are bridged by the phenolic oxygen of $(L^2)^-$ and an acetate group in the syn-syn mode: the Ni1--Ni2 intermetallic separation is 3.254(1) Å. The nickel bound to the iminic pendant arm (Ni1) has a four-coordinate geometry with short Ni−N and Ni−O bond distances (1.843(7)−1.963(7) Å). The configuration around the metal can be regarded as a square plane showing a slight distortion to a tetrahedron: the dihedral angle between the least-squares plane defined by Ni1, N1, and N2 and the plane defined by Ni1, O1, and O2 is 15.4°. Ni2 bound to the aminic pendant arm has a six-coordinate geometry with further coordination of an acetate group in the chelating mode. Thus, the molecule has a {4/6} coordination number set. The O4−Ni2−O5 angle in the chelating acetate is small (59.8(2)°). In contrast, the O3−Ni2−O4, O3−Ni2−N3, and O5−Ni2−N3 angles are enlarged (98.3(3), 101.2(2), and 100.4-(3)°, respectively). When we presume the donor atoms O1, N3, N4, and O4 to form an equatorial plane about Ni2, the bridging acetate group coordinates to an axial site of Ni2 through O3 and to an equatorial site of Ni1 through O2. Because of this, the $\{NiN_2O_2\}$ entity of the planar Ni1 is not coplanar with the conjugated part of $(L^2)^-$. This is reflected by the nonplanar

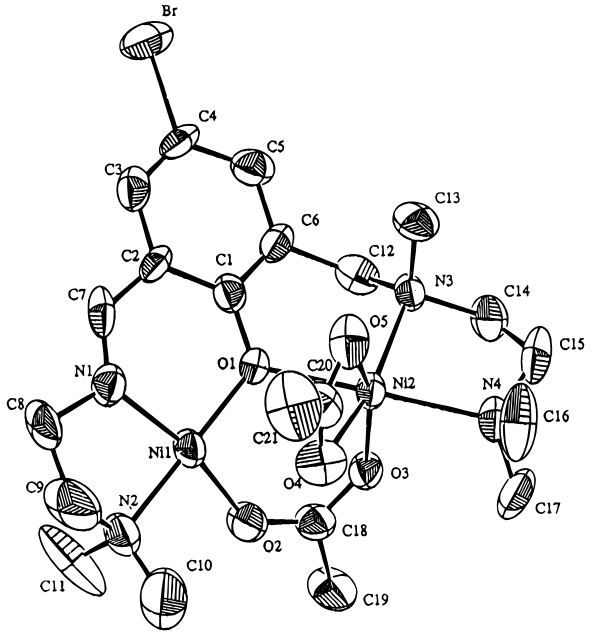

Figure 3. ORTEP view of $[Ni_2(L^2)(AcO)_2]BPh_4$ (**4**).

Table 4. Relevant Bond Distances (Å) and Angles (deg) for **4**

	Distances		
Ni1−O1	1.858(5)	Ni1−O2	1.862(6)
Ni1−N1	1.843(7)	Ni1−N2	1.963(7)
Ni2−O1	2.118(5)	Ni2−O3	2.014(5)
Ni2−O4	2.178(7)	Ni2−O5	2.097(6)
Ni2−N3	2.058(6)	Ni2−N4	2.158(7)
Ni1--Ni2	3.254(1)		
	Angles		
O1−Ni1−O2	93.3(2)	O1−Ni1−N1	95.1(3)
O1−Ni1−N2	176.7(3)	O2−Ni1−N1	163.0(3)
O2−Ni1−N2	88.1(3)	N1−Ni1−N2	84.4(3)
O1−Ni2−O3	82.8(2)	O1−Ni2−O4	87.3(2)
O1−Ni2−O5	91.2(2)	O1−Ni2−N3	90.3(2)
O1−Ni2−N4	171.0(3)	O3−Ni2−O4	98.3(3)
O3−Ni2−O5	157.6(3)	O3−Ni2−N3	101.2(2)
O3−Ni2−N4	90.0(3)	O4−Ni2−O5	59.8(2)
O4−Ni2−N3	159.9(3)	O4−Ni2−N4	99.1(3)
O5−Ni2−N3	100.4(3)	O5−Ni2−N4	97.5(3)
N3−Ni2−N4	85.8(3)	Ni1−O1−Ni2	109.7(3)

configuration about the phenolic oxygen O1; the sum of the bite angles C1−O1−Ni1, C1−O1−Ni2, and Ni1−O1−Ni is 356.3°.

Complex 5. An ORTEP view of $[Ni_2(L^2)(NCS)_3(MeOH)]$ (**5**) is shown in Figure 4. Selected bond distances and angles are given in Table 5.

X-ray crystallography indicates that the aminic pendant arm adopts an "out-of-plane" chelating mode in this complex. The two Ni ions are bridged by the phenolic oxygen of $(L^2)^-$ and an isothiocyanate nitrogen; the Ni--Ni separation is 3.142(2) Å. Ni1 bound to the iminic pendant arm has a five-coordinate structure with O1, N1 and N2 of $(L^2)^-$, N5 of a monodentate isothiocyanate group, and N6 of the bridging isothiocyanate group. The geometry about the metal is best depicted as a square pyramid where the basal plane is formed by O1, N1, N2, and N6. The equatorial bond distances vary from 1.961(7) to 2.108(7) Å. The axial Ni−N5 bond is relatively short (1.991(7) Å). Ni1 deviates 0.373 Å from the basal least-squares plane toward N5. Ni2 bound to the aminic pendant arm has a pseudo octahedral geometry with further coordination of a methanol molecule. Thus, this complex has a {5/6} coordination number set. The equatorial plane about Ni2 is formed by

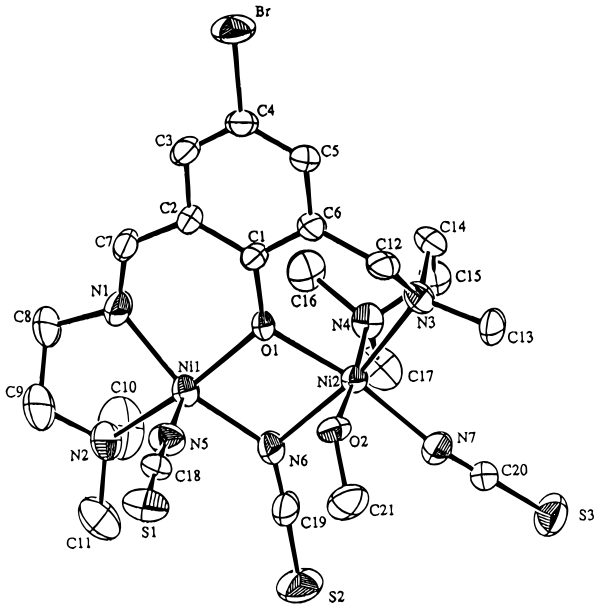

Figure 4. ORTEP view of $[Ni_2(L^2)(NCS)_3(MeOH)]$ (**5**).

Table 5. Relevant Bond Distances (Å) and Angles (deg) for **5**

	Distances		
Ni1−O1	2.013(4)	Ni1−N1	1.961(7)
Ni1−N2	2.108(7)	Ni1−N5	1.991(7)
Ni1−N6	2.039(7)	Ni2−O1	2.044(5)
Ni2−O2	2.159(5)	Ni2−N3	2.100(6)
Ni2−N4	2.113(6)	Ni2−N6	2.170(6)
Ni2−N7	2.025(7)	Ni1--Ni2	3.142(2)
	Angles		
O1−Ni1−N1	89.8(3)	O1−Ni1−N2	165.2(3)
O1−Ni1−N5	95.6(3)	O1−Ni1−N6	82.9(2)
N1−Ni1−N2	83.8(3)	N1−Ni1−N5	105.0(3)
N1−Ni1−N6	152.9(3)	N2−Ni1−N5	99.0(4)
N2−Ni1−N6	96.7(2)	N5−Ni1−N6	101.7(3)
O1−Ni2−O2	78.7(2)	O1−Ni2−N3	90.4(2)
O1−Ni2−N4	96.1(2)	O1−Ni2−N6	79.0(2)
O1−Ni2−N7	168.4(3)	O2−Ni2−n3	92.9(2)
O2−Ni2−N4	174.6(2)	O2−Ni2−N6	86.6(2)
O2−Ni2−N7	91.5(3)	N3−Ni2−N4	85.9(3)
N3−Ni2−N6	169.3(3)	N3−Ni2−N7	96.3(3)
N4−Ni2−N6	93.6(3)	N4−Ni2−N7	93.9(3)
N6−Ni2−N7	94.4(3)	Ni1−O1−Ni2	101.5(2)

O1 and N3 of $(L^2)^-$, N6 of the bridging isothiocyanate group, and N7 of the monodentate isothiocyanate group. The axial sites are occupied by the terminal nitrogen N4 of the pendant arm and a methanol oxygen O2. The Ni2−O2 bond (2.159(5) Å) is relatively long among the Ni2-to-ligand bonds.

Properties. (a) IR Spectra. Complex **1** shows the antisymmetric and symmetric vibrations of the acetate group at 1570 and 1460 cm^{-1}, respectively. The small separation between the two vibrations suggests a bidentate mode for the acetate group.[25] Similarly, a small separation between the antisymmetric and symmetric vibrations of the acetate group is observed for **2**−**4**, all of which have at least one bidentate (bridging or chelating) acetate group as discussed above. Each of **1**, **3**, and **5** shows two distinct ν(CN) modes for the NCS^- group (2080 and 2022 cm^{-1} for **1**, 2075 and 2025 cm^{-1} for **2**, and 2080 and 1980 cm^{-1} for **5**). This is in harmony with the X-ray crystallographic results indicating that one bridging and one monodentate thiocyanate group is involved in each crystal. The higher frequency band can be assigned to the monodentate

(25) Deacon, G. B.; Phillips, R. J. *Coord. Chem. Rev.* **1980**, *33*, 227.

isothiocyanate group and the lower frequency band to the bridging isothiocyanate group.[26] The corresponding ν(CS) modes are obscured by ligand vibrations. **2** and **4** both have an intense vibration at 710 cm^{-1} that is characteristic of the tetraphenylborate ion. All the complexes show the ν(C═N) mode of the azomethine group at ∼1650 cm^{-1}.

(b) Visible Spectra. Complexes **1**, **3**, and **5** are nonelectrolytes in dichloromethane, while **2** and **4** have a molar conductance typical of 1:1 electrolytes in this solvent (46 and 45 S cm^2 mol^{-1}, respectively).[27] Each complex shows a close resemblance between absorption (in dichloromethane) and reflectance spectra. Numerical data from the absorption spectra are given in the Experimental Section.

Complex **1** exhibits two distinct absorption bands at 610 and 880 nm and a weaker band near 780 nm. A similar spectrum is observed for **3** that has a core with a {6/6} coordination number set. If we assume O_h symmetry for the two nickel ions of **1** and **3**, the two bands at ∼610 and ∼880 nm can be assigned to the spin-allowed d−d transitions $^3T_{2g} \leftarrow {}^3A_{2g}$ and $^3T_{1g} \leftarrow {}^3A_{2g}$, respectively.[28,29] The weak band near 780 nm can be assigned to the spin-forbidden transition $^1E_g \leftarrow {}^3A_{2g}$. Complexes **2** and **5**, having a core with a {5/6} coordination number set, exhibit two distinct absorption bands at ∼660 and ∼880 nm along with a weaker band at ∼780 nm. The spectrum of **4** is characterized by a discernible shoulder near 500 nm that is typical of a planar nickel(II) ion.[29] Because of this absorption, **4** assumes a brown color, whereas the other complexes are green.

(c) Magnetism. The room-temperature magnetic moments of **1**−**3** (per one Ni) fall in the range 3.10−3.15 μ_B. The magnetic moments gradually decrease with decreasing temperature, suggesting the presence of an antiferromagnetic interaction between a pair of nickel(II) ions. The χ_A vs T and μ_{eff} vs T curves for **1** are given in Figure 5.

Magnetic analyses were carried out by using the magnetic susceptibility expression based on the isotropic Heisenberg model ($\boldsymbol{H} = -2JS_1S_2$, $S_1 = S_2 = 1$):

$$\chi_A = (Ng^2\beta^2/3kT)[5 + \exp(-4J/kT)]/[5 + 3\exp(-4J/kT) + \exp(-6J/kT)] + N\alpha \quad (1)$$

where N is the Avogadro number, β is the Bohr magneton, k is the Boltzman constant, g is the Zeeman splitting constant, T is the absolute temperature, J is the exchange integral, and $N\alpha$ is the temperature-independent paramagnetism. The cryomagnetic property of **1** can be simulated by this expression as indicated by the solid curve, using the magnetic parameters $g = 2.21$, $J = -0.8$ cm^{-1}, and $N\alpha = 200 \times 10^{-6}$ cm^3 mol^{-1}. Similarly, negative exchange integrals are obtained for **2** (−1.0 cm^{-1}) and **3** (−1.7 cm^{-1}).

The magnetic moment of **5** is 3.25 μ_B at room temperature and gradually increases with decreasing temperature up to a maximum of 3.56 μ_B near 20 K (Figure 5). Evidently a ferromagnetic interaction operates between the pair of nickel ions. With further decreasing temperature, the magnetic moment tends to drop probably due to a secondary effect such as zero-field splitting of $S_{Ni} = 1$ or interdimer antiferromagnetic

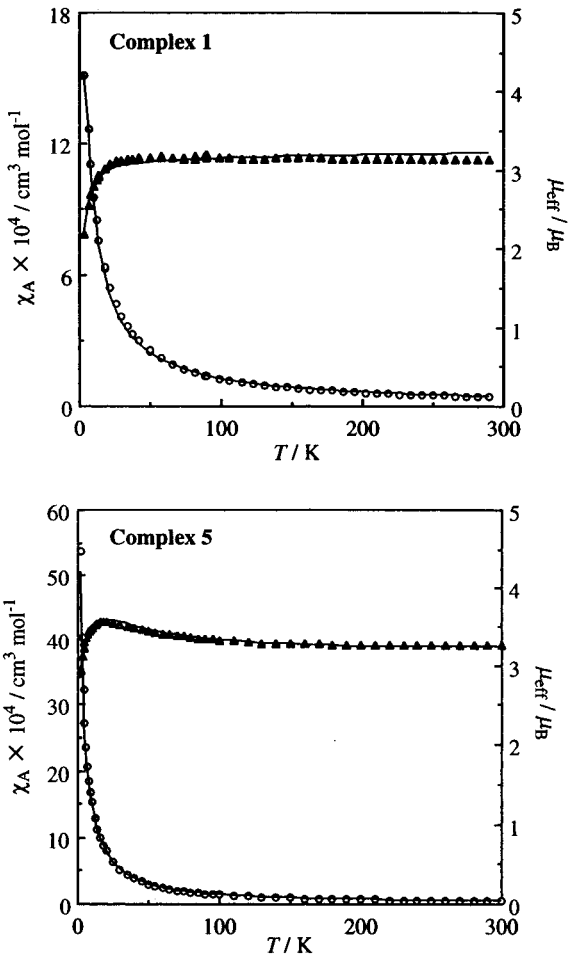

Figure 5. χ_A vs T (▲) and μ_{eff} vs T (○) curves for **1** and **5**.

interaction. Magnetic simulations based on the expression containing the correction term Θ for the secondary effect

$$\chi_A = [Ng^2\beta^2/3k(T - \Theta)][5 + \exp(-4J/kT)]/[5 + 3\exp(-4J/kT) + \exp(-6J/kT)] + N\alpha \quad (2)$$

gave a good fitting as indicated in Figure 5, using the magnetic parameters of $g = 2.17$, $J = +10$ cm^{-1}, $\Theta = -1.5$ K, and $N\alpha = 200 \times 10^{-6}$ cm^3 mol^{-1}. Magnetostructural correlations have been extensively studied for dinuclear copper(II) complexes, and the significance of the Cu−X−Cu angle in a dibridged system and the coplanarity about the bridging oxygen in determining the sign of the exchange integral are well documented.[31−33] A similar magnetostructural study has been conducted for dinuclear nickel(II) complexes.[34] For the present dinuclear nickel(II) complexes, however, we cannot identify any dominant factor contributing to the positive (for **5**) or negative (for **1**−**3**) exchange integral from inspection of their crystal structures.

The magnetic moment of **4** is 3.31 μ_B per molecule at room temperature, and the moment is practically independent of temperature down to 10 K. This, together with X-ray crystallographic and visible spectral data, shows that **4** is evidently a

(26) Nakamoto, K. *Infrared Spectra of Inorganic and Coordination Compounds*; Wiley Interscience: New York, 1970; p 187.
(27) Geary, W. J. *Coord. Chem. Rev.* **1971**, *7*, 81.
(28) Sacconi, L. *Coord. Chem. Rev.* **1966**, *1*, 192.
(29) Yamada, S. *Coord. Chem. Rev.* **1966**, *1*, 415.
(30) Bosnich, B. *J. Am. Chem. Soc.* **1968**, *90*, 627.
(31) Melnik, M. *Coord. Chem. Rev.* **1982**, *42*, 259.
(32) Cairns, C. J.; Busch, D. H. *Coord. Chem. Rev.* **1986**, *69*, 1.
(33) Handa, M.; Koga, N.; Kida, S. *Bull. Chem. Soc. Jpn.* **1988**, *61*, 3853.
(34) Nanda, K. K.; Das, R.; Thompson, L. K.; Venkastsubramanian, K.; Paul, P.; Nag, K. *Inorg. Chem.* **1994**, *33*, 1188.

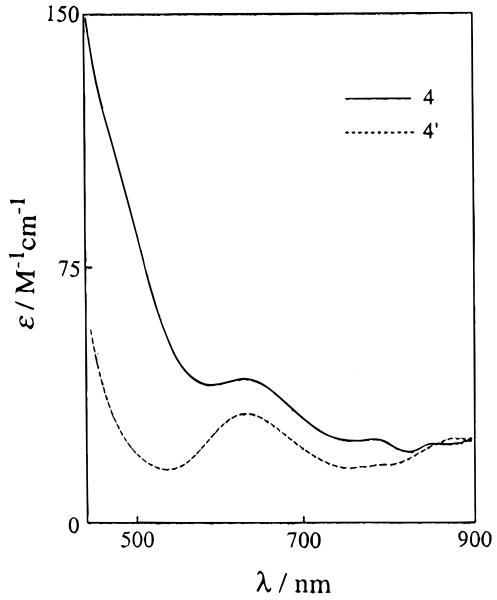

Figure 6. Visible spectra of **4** and **4′** in dichloromethane.

mixed-spin complex having one low-spin ($S = 0$) and one high-spin ($S = 1$) nickel(II) ion.

Urea Adducts. Urea adducts of dinuclear nickel complexes are of current interest because of relevance to the urease active site.[10] In this study, we have found that **4** and **5** form the urea adducts $[Ni_2(L^2)(AcO)_2(urea)]BPh_4$ (**4′**) and $[Ni_2(L^2)(NCS)_3$-(urea)] (**5′**), respectively. Urea binding through its oxygen in these urea adducts is inferred from new IR bands at 3550−3300 and 1660 cm^{-1} which are assigned to the ν(N−H) and ν(C═O) modes, respectively. In Figure 6 is shown the visible spectrum of **4′** together with the spectrum of the precursor complex **4**. The discernible shoulder near 500 nm of **4**, typical of planar Ni^{II}, disappears in the spectrum of **4′**. This fact means that the urea binding occurs at the four-coordinate Ni center. The room-temperature magnetic moment of **4′** is 3.29 μ_B per one nickel (4.65 μ_B per molecule), clearly indicating that both nickel ions are paramagnetic. The urea adduct resembles **4** in cryomagnetic properties; the μ_{eff} increases with decreasing temperature up to a maximum value of 3.69 μ_B at 8.1 K and then decreases below this temperature. Magnetic simulations based on eq 2 gave the best-fit parameters $g = 2.25$, $J = +4.0$ cm^{-1}, $\Theta = -0.7$ K, and $N\alpha = 200 \times 10^{-6}$ cm^3 mol^{-1}.

The spectral resemblance between **5′** and **5** (see Experimental Section) suggests a similarity in their dinuclear cores. This was proved by X-ray crystallography. An ORTEP view of **5′** is shown in Figure 7 together with the numbering scheme. Relevant bond distances and angles are given in Table 6.

The urea adduct **5′** retains the dinuclear core of **5** bridged by the phenolic oxygen O1 of $(L^2)^-$ and the isothiocyanate nitrogen N6. The aminic pendant arm of $(L^2)^-$ adopts a similar out-of-plane chelating mode toward N2. One essential difference between **5′** and **5** is seen in the sixth exogenous ligand of Ni2; this is urea in **5′** while it is methanol in **5**. The five-coordinate Ni1 at the iminic site shows little change on urea binding; the average Ni1-to-ligand bond distance of **5′** (2.026 Å) is comparable to that of **5** (2.022 Å). Ni2 at the aminic site shows a slight change in its six-coordinate environment on urea binding. The average of the Ni2-to-ligand bond distances in **5′** is 2.110 Å, which is short relative to that of **5** (2.168 Å). The Ni2−O2(urea) bond distance is 2.125(5) Å, which is common for a Ni−O(urea) distance.[10] The Ni−O(urea) bond distance is short

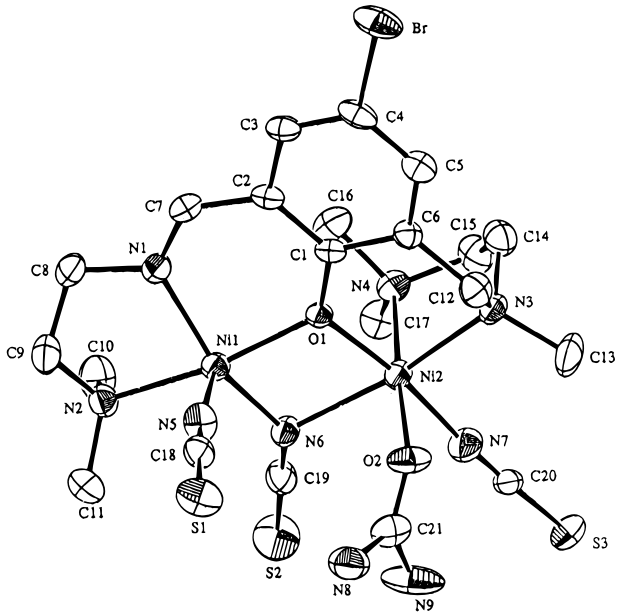

Figure 7. ORTEP view of $[Ni_2(L^2)(NCS)_3(urea)]$ (**5′**).

Table 6. Relevant Bond Distances (Å) and Angles (deg) for **5′**

	Distances		
Ni1−O1	1.992(4)	Ni1−N1	1.981(5)
Ni1−N2	2.107(5)	Ni1−N5	1.975(6)
Ni1−N6	2.077(5)	Ni2−O1	2.058(4)
Ni2−O2	2.125(5)	Ni2−N3	2.094(5)
Ni2−N4	2.158(6)	Ni2−N6	2.197(5)
Ni2−N7	2.030(6)	Ni1--Ni2	3.155(2)
	Angles		
O1−Ni1−N1	90.3(2)	O1−Ni1−N2	166.6(2)
O1−Ni1−N5	98.2(2)	O1−Ni1−N6	83.5(2)
N1−Ni1−N2	83.4(2)	N1−Ni1−N5	99.2(2)
N1−Ni1−N6	148.5(2)	N2−Ni1−N5	94.4(2)
N2−Ni1−N6	95.8(2)	N5−Ni1−N6	112.2(2)
O1−Ni2−O2	87.0(2)	O1−Ni2−N3	90.3(2)
O1−Ni2−N4	93.1(2)	O1−Ni2−N6	79.0(2)
O1−Ni2−N7	172.8(2)	O2−Ni2−N3	91.4(2)
O2−Ni2−N4	176.3(2)	O2−Ni2−N6	87.7(2)
O2−Ni2−N7	90.5(2)	N3−Ni2−N4	84.9(2)
N3−Ni2−N6	169.3(2)	N3−Ni2−N7	96.5(2)
N4−Ni2−N6	95.9(2)	N4−Ni2−N7	89.8(2)
N6−Ni2−N7	94.1(2)	Ni1−O1−Ni2	102.3(2)

compared with the Ni−O(methanol) bond of **5** (2.159(5) Å). The Ni1--Ni2 separation in **5′** is 3.155(2) Å.

The μ_{eff} vs T behavior of **5′** is essentially similar to those of **5** and **4′**, indicating a ferromagnetic spin exchange within a molecule. Magnetic simulations by means of eq 2 gave the following best-fit parameters: $g = 2.12$, $J = +10.0$ cm^{-1}, $\Theta = -0.7$ K, and $N\alpha = 200 \times 10^{-6}$ cm^3 mol^{-1}. Magnetic studies for urease have provided conflicting results for magnetic exchange interactions.[35−37] The present magnetic studies for the dinuclear nickel complexes (**1**−**5**) and the urea adducts (**4′** and **5′**) suggest that the magnetic interaction in dinuclear nickel is complicatedly affected by various factors to give a positive or negative exchange integral by a slight structural change.

It must be emphasized that urea adduct formation does not occur for **1**−**3**. **3** has a core with a {6/6} coordination number set, and **1** probably has a similar core. The coordinative

(35) Clark, P. A.; Wilcox, D. E. *Inorg. Chem.* **1989**, *28*, 1326.
(36) Finnegan, M. G.; Kowal, A. T.; Werth, M. T.; Clark, P. A.; Wilcox, D. E.; Johnson, M. K. *J. Am. Chem. Soc.* **1991**, *113*, 4030.
(37) Day, E. P.; Peterson, J.; Sendova, M. S.; Todd, M. J.; Hausinger, E. P. *Inorg. Chem.* **1993**, *32*, 634.

saturation of two nickel centers explains why these two complexes cannot bind urea. Complex **2** has a core with a {5/6} coordination number set but cannot bind urea. In relating to this, it must be pointed out that dinuclear Mn(II) complexes of $(L^1)^-$ and $(L^2)^-$ prefer similar asymmetric cores with {5/6} coordination number sets.[15,37] It is plausible that when one metal is six-coordinate, the other metal cannot take a six-coordinate geometry owing to intracore strain within $(L^1)^-$ and $(L^2)^-$. That is, the core of with a {5/6} coordination number set is practically saturated for weakly donative ligands such as urea. Complex **4** has an unsaturated core with a {4/6} coordination number set to allow urea binding at the four-coordinate Ni center. In the case of **5**, with a core with a {5/6} coordination number set, the methanol ligand is more or less released and the resulting $[Ni_2(L^2)(NCS)_3]$ with a {5/5} coordination number set binds urea instead of the methanol.

Acknowledgment. This work was supported by a Grant-in-Aid for Scientific Research (No. 09440231) from the Ministry of Education, Science, and Culture of Japan. Thanks are also expressed to the British Council for support.

Supporting Information Available: X-ray crystallographic files, in CIF format, for **2**, **3**, **4**, **5**, and **5′** are available on the Internet only. Access information is given on any current masthead page.

IC971209P